Efficient Computation of Casimir Interactions between Arbitrary 3D Objects

Citation: Efficient Computation of Casimir Interactions between Arbitrary 3D Objects M. T. Homer Reid, Alejandro W. Rodriguez, Jacob White, and Steven G. Johnson, Phys. Rev. Lett. 103, 040401 (2009), DOI:10.1103/PhysRevLett.103.040401

As Published: http://dx.doi.org/10.1103/PhysRevLett.103.040401

Publisher: The American Physical Society

Persistent URL: http://hdl.handle.net/1721.1/49435

Version: Author's final manuscript: final author's manuscript post peer review, without publisher's formatting or copy editing

Efficient Computation of Casimir Interactions between Arbitrary 3D Objects

M. T. Homer Reid[1,2*†], Alejandro W. Rodriguez[1], Jacob White[2,3], and Steven G. Johnson[2,4]
[1] *Department Of Physics, Massachusetts Institute of Technology, Cambridge, MA 02139, USA*
[2] *Research Laboratory of Electronics, Massachusetts Institute of Technology, Cambridge, MA 02139, USA*
[3] *Department of Electrical Engineering and Computer Science, Massachusetts Institute of Technology, Cambridge, MA 02139, USA*
[4] *Department Of Mathematics, Massachusetts Institute of Technology, Cambridge, MA 02139, USA*
(Dated: June 10, 2009)

We introduce an efficient technique for computing Casimir energies and forces between objects of arbitrarily complex 3D geometries. In contrast to other recently developed methods, our technique easily handles non-spheroidal, non-axisymmetric objects and objects with sharp corners. Using our new technique, we obtain the first predictions of Casimir interactions in a number of experimentally relevant geometries, including crossed cylinders and tetrahedral nanoparticles.

PACS numbers: 03.70.+k, 12.20.-m, 42.50.Lc, 03.65.Db

Since the dawn of the modern era of precision Casimir-force measurements some 10 years ago [1], Casimir forces have been measured in an increasingly wide variety of experimental geometries, including plate-plate [2], sphere-plate [3], sphere-comb [4], and cylinder-cylinder [5] configurations. A recent experiment [6] finds evidence of Casimir interactions in a commercially fabricated MEMS device, and there is every reason to believe that accurate modeling of Casimir forces in complex geometries will be a critical ingredient in the design of future commercial MEMS technologies [7–9].

Theoretical developments have largely failed to keep pace with this rapidly advancing experimental reality. Until recently, theoretical considerations were restricted to simple models in highly idealized geometries [10], such as infinite parallel plates or infinite parallel cylinders. Techniques for predicting Casimir forces in more general geometries are clearly needed if theory is to confront the growing wealth of experimental Casimir data and the design challenges of future MEMS devices.

Important recent progress on general methods has been made by a number of authors [11–15]. Rodriguez *et. al.* [11] applied standard techniques of computational electromagnetics to develop a method capable of predicting Casimir forces between arbitrary *two-dimensional* objects, i.e. infinitely extended objects of arbitrary 2D cross section. Emig *et. al.* (EGJK) [12] demonstrated an efficient algorithm for predicting Casimir energies of interaction between compact 3D objects of *spheroidal* or *nearly-spheroidal* shape. Both of these techniques have since been applied to predictions of Casimir interactions in new geometries [16–18]. To date, however, a practical computational scheme for predicting Casimir forces between arbitrary non-spheroidal three-dimensional objects has remained elusive.

In this work, inspired by the ideas of Refs. 11 and 12, we introduce a new technique for calculating Casimir forces between objects of arbitrary 3D shapes, including efficient handling of non-spheroidal, non-axisymmetric objects and objects with sharp corners. As an immediate application of our method, we present the first predictions of Casimir interactions in a number of experimentanlly relevant geometries, including crossed cylindrical capsules [5] and tetrahedral nanoparticles [21, 22].

The method. The starting point of the EGJK method

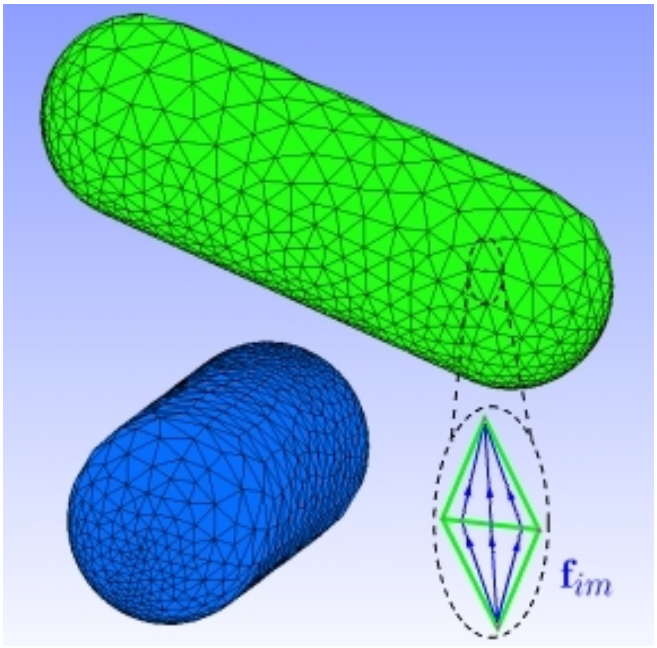

FIG. 1: Surfaces of compact conducting objects are discretized [19] into planar triangles, which are used to construct localized vector-valued basis functions describing the surface current distribution. As shown in the inset, each basis function describes currents flowing from a vertex of one triangle to the opposite vertex of an adjacent triangle, and vanishes on all other triangles [20].

*Electronic address: homereid@mit.edu
†URL: http://www.mit.edu/~homereid

is a path-integral expression [23] for the Casimir energy of perfectly-conducting compact objects:

$$\mathcal{E} = -\frac{\hbar c}{2\pi}\int_0^\infty d\kappa \log\frac{\mathcal{Z}(\kappa)}{\mathcal{Z}_\infty(\kappa)}, \tag{1}$$

$$\mathcal{Z}(\kappa) = \int \mathcal{D}\mathbf{J}(\mathbf{x})\, e^{-\frac{1}{2}\int d\mathbf{x}\int d\mathbf{x}'\,\mathbf{J}(\mathbf{x})\cdot\boldsymbol{\mathcal{G}}_\kappa(\mathbf{x},\mathbf{x}')\cdot\mathbf{J}(\mathbf{x}')} \tag{2}$$

where the functional integration extends over all possible current distributions $\mathbf{J}(\mathbf{x})$ on the surfaces of the objects and where $\boldsymbol{\mathcal{G}}_\kappa = \left[\mathbf{1} + \frac{1}{\kappa^2}\nabla\otimes\nabla'\right]\frac{e^{-\kappa|\mathbf{x}-\mathbf{x}'|}}{4\pi|\mathbf{x}-\mathbf{x}'|}$ is the dyadic Green's function at (Wick-rotated) frequency $-i\omega = c\kappa$. $\mathcal{Z}_\infty$ in (1) is $\mathcal{Z}$ computed with all objects removed to infinite separation [32].

Following EGJK, to obtain a tractable expression for $\mathcal{Z}$ for a given collection of N_o objects we now proceed to expand the current distribution in a discrete set of basis functions, $\mathbf{J}(\mathbf{x}) = \sum J_{im}\mathbf{f}_{im}(\mathbf{x})$, where $i = 1\cdots N_o$ ranges over the objects in the geometry and $m = 1\cdots N_i$ runs over a set of N_i expansion functions defined for the ith object. With this expansion we have

$$\mathcal{Z}(\kappa) = \mathcal{J}\int\prod dJ_{im}\, e^{-\frac{1}{2}\sum J_{im}\mathbf{M}^{(\kappa)}_{im,jn}J_{jn}} \tag{3}$$

$$= (2\pi)^{n/2}\mathcal{J}\cdot[\det\mathbf{M}(\kappa)]^{-1/2} \tag{4}$$

and (1) becomes

$$\mathcal{E} = +\frac{\hbar c}{2\pi}\int_0^\infty d\kappa\, \log\frac{\det\mathbf{M}(\kappa)}{\det\mathbf{M}_\infty(\kappa)} \tag{5}$$

where we have evaluated the multiple Gaussian integral in (3) using standard path-integration techniques [24]. Here the elements of the matrix $\mathbf{M}(\kappa)$ are the interactions between the basis functions, $\mathbf{M}_{\alpha\beta}(\kappa) = \iint \mathbf{f}_\alpha\cdot\boldsymbol{\mathcal{G}}_{\boldsymbol{\kappa}}\cdot\mathbf{f}_\beta\, d\mathbf{x}\, d\mathbf{x}'$, and $\mathcal{J}$ in (3) is the (constant) Jacobian of the transformation $\mathcal{D}\mathbf{J}\to\prod dJ_{im}$, which cancels in the ratio (5).

EGJK took the expansion functions $\mathbf{f}_{im}$ to be proportional to the spherical multipole moments $\{Q^i_{E,lm}, Q^i_{M,lm}\}$ of the ith object. Although this choice leads to rapidly convergent and even analytically tractable series for *spherical* objects, it is not of practical use for general geometries, as the spherical multipole expansion must be carried to high orders to represent source distributions on highly non-spherical objects. Ref. 25, for example, demonstrated poor convergence rates for spherical-harmonic representations of elongated objects and objects with corners or cusps.

A more general strategy is to discretize the surfaces of the objects into planar triangles, as depicted in Figure 1, and to introduce *localized* basis functions in the spirit of finite-element and boundary-element methods. Following standard practice in computational electromagnetics [20], we choose basis functions defined on pairs of adjacent triangles. As indicated in the inset of Figure 1, to the mth internal edge in the surface discretization of object i we associate a localized basis function $\mathbf{f}_{im}$, which describes currents flowing on the two triangles that share that edge and vanishes on all other triangles. The matrix elements $\mathbf{M}_{\alpha\beta}$ reduce to finite surface integrals over plane triangles, the evaluation of which is greatly facilitated by the elegant methods of Ref. 26, and the overall accuracy of the computation may be systematically improved, at greater computational expense, by reducing the size of the triangles in the surface mesh. A further virtue of this choice of basis functions is that it eliminates the unwieldy distinction between interior and exterior fields in [12].

Casimir Energy. To compute the energy of interaction of our objects we write

$$\log\frac{\det\mathbf{M}}{\det\mathbf{M}_\infty} = \sum_{n=1}^N\Big\{\log\lambda_n - \log\lambda_n^\infty\Big\} \tag{6}$$

where $\{\lambda_n\}, \{\lambda_n^\infty\}$ are the eigenvalues of $\mathbf{M}, \mathbf{M}_\infty$.

Casimir Force. The z-directed force on the ith object in our geometry is obtained by differentiating (5) with respect to displacement of that object:

$$\mathcal{F}_{z,i} = -\frac{\hbar c}{2\pi}\int_0^\infty d\kappa\,\frac{\partial}{\partial z_i}\ln\frac{\det\mathbf{M}(\kappa)}{\det\mathbf{M}_\infty(\kappa)}. \tag{7}$$

The integrand may be conveniently evaluated using the identity [27]

$$\frac{\partial}{\partial z_i}\ln\det\mathbf{M} = \mathrm{Tr}\left\{\mathbf{M}^{-1}\cdot\frac{\partial\mathbf{M}}{\partial z_i}\right\} = \sum_{n=1}^N\alpha_n$$

where $\{\alpha_n\}$ are the eigenvalues of the *generalized* eigenvalue problem

$$\frac{\partial\mathbf{M}}{\partial z_i}\cdot\mathbf{v} = \alpha\mathbf{M}\cdot\mathbf{v}. \tag{8}$$

The κ integrals in (5) and (7) may be evaluated using standard numerical quadrature techniques.

The dimension of the matrix $\mathbf{M}$ is the number of basis functions in our expansion of the surface current distribution, which in turn is proportional to the number of triangles in our surface discretization (see Figure 1). For matrices of moderate dimension, $N \lesssim 5000$, corresponding to moderately fine mesh discretizations (sufficient for accurate treatment of all geometries considered here), the eigenvalues in (6) and (8) may be computed using direct methods in $\mathcal{O}(N^3)$ time. For finer meshes it may be possible to use iterative eigenvalue solvers and matrix sparsification techniques [28–30] to reduce the complexity to $\mathcal{O}(N\ln N)$; this will be discussed in a subsequent publication.

Results. We now apply our technique to the prediction of Casimir interactions in a number of 3D geometries.

Casimir energy of identical spheres, parallel capsules, and crossed capsules. Figure 2 shows plots of Casimir

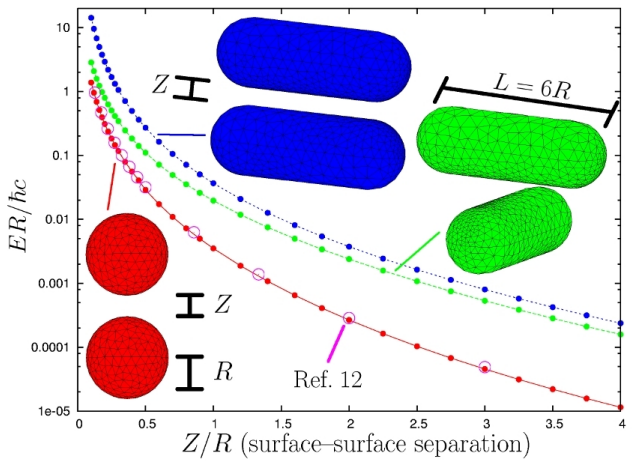

FIG. 2: Casimir energy vs. separation distance for three pairs of perfectly conducting objects: identical spheres (red curve), identical capsules with parallel axes (blue curve), and identical capsules with perpendicular axes (green curve). The hollow circles represent the sphere-sphere data of Ref. 12.

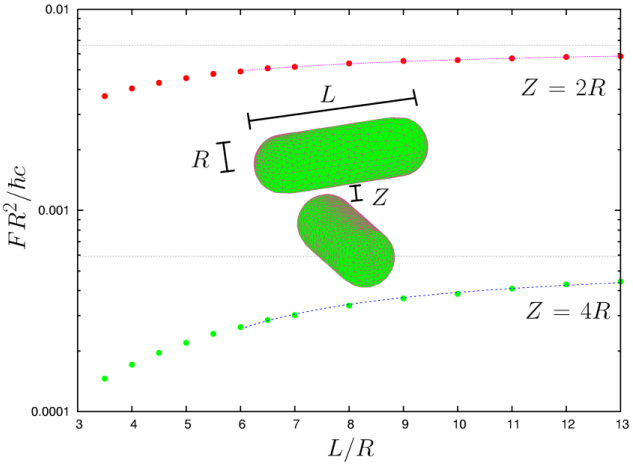

FIG. 3: Magnitude of attractive Casimir force between crossed capsules of radius R as a function of capsule length, for surface–surface separations $Z = 2R$ and $Z = 4R$. The dashed lines denote the asymptotic ($L \to \infty$) limits of the force, as roughly extrapolated from our finite-L data. The solid lines are fits of the large-L data to the form $a + b/L$, although our data are insufficient to establish the precise asymptotic L-dependence of the force.

energy versus separation distance for three pairs of perfectly conducting objects: identical spheres of radius R, identical capsules with parallel axes, and identical capsules with perpendicular axes ("crossed capsules.") (A "capsule" is a cylinder of radius R with hemispherical endcaps, of total length $L = 6R$ in this case.) The energy curve for the crossed capsules interpolates between the curve for the spheres at short distances and the curve for the parallel capsules at large distances. We may understand this result as follows: At short distances, the interaction is dominated by contributions from the portions of the surfaces that lie in closest proximity to each other. For the crossed capsules, this region of nearest proximity is restricted to a length $\sim R$ around the centers of the capsules and hence exhibits the same scaling as the region of nearest proximity for the two spheres in the short-distance limit. In contrast, for parallel capsules, the strongly-interacting region extends down the entire length of the capsule and hence scales with an additional factor of L at short distances. At large distances, the interaction becomes pointlike and the energy of interaction between identical capsules becomes independent of the orientation.

Casimir Force vs. Length For Crossed Capsules. The Casimir force between crossed cylinders, in the limit in which the length L of the cylinders is much longer than their surface–surface separation Z, is experimentally accessible [5] and interesting in its own right as a finite interaction between effectively infinite objects. Figure 3 plots the magnitude of the attractive Casimir force between crossed metallic capsules of radius R, at fixed surface–surface separations of $Z = 2R$ and $Z = 4R$, as a function of the capsule length L. In the limit $L \to \infty$ our capsules become infinite cylinders and the force approaches a Z-dependent constant (denoted by the dashed lines in the figure.)

An interesting question is how rapidly the force approaches the infinite-cylinder limit as $L \to \infty$ at fixed Z. A numerical determination of the precise asymptotic L-dependence of the force requires an iterative fast-solver version of our method that is capable of handling matrices $\mathbf{M}$ of larger dimension; this extension will be discussed in a future publication.

Tetrahedral nanoparticles. Several groups have succeeded in producing tetrahedral nanoparticles of dimensions $\sim$ 10–50 nm [21, 22], and Casimir forces may dominate the interactions between electrostatically neutral particles of this type. Our method allows the first predictions of Casimir interactions between perfectly conducting tetrahedral particles. (In a real system with particles of these sizes, the finite conductivity of the metals cannot be neglected. We are currently implementing an extension of our method to treat materials of arbitrary electrical properties, including imperfect metals, dielectrics, and magnetic materials. Even for the idealization of perfectly conducting nanoparticles, however, it is interesting to analyze the orientation dependence of the Casimir energy, as well as to demonstrate the practical ability of our method to treat geometries with sharp corners and non-axisymmetric shapes.) Figure 4 depicts a contour plot of Casimir energy vs. orientation angles for two perfectly conducting tetrahedra originally separated by a distance $D = 2L$ in the y direction, where L is the tetrahedron edge length. To one of the tetrahedra we apply a rotation through an angle φ about the z axis followed by a rotation through an angle θ about the y axis; the fixed origin

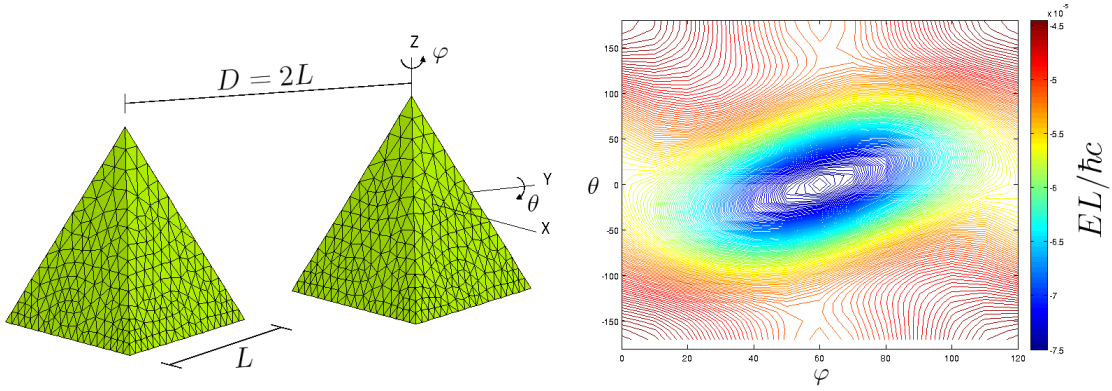

FIG. 4: Contour plot of Casimir energy vs. orientation angles for tetrahedral nanoparticles separated by a distance $D = 2L$.

of these rotations, depicted as the origin of the coordinate axes in Figure 4, is the point lying a distance $H/2$ below the apex of the tetrahedron, where $H = \sqrt{3}L/2$ is the height of the tetrahedron. The contour plot reveals a clear minimum at (θ, ϕ)=(0,60°), corresponding to the closest approach of a vertex of the base of the rotated tetrahedron to the unrotated tetrahedron, as might be expected for an attractive interaction.

Conclusion. In conclusion, we have developed a general method for computing Casimir energies and forces between objects of arbitrary three-dimensional shapes, enabling efficient treatment of non-spheroidal, non-axisymmetric objects and objects with sharp corners. Using our method, we have predicted Casimir interactions in a variety of experimentally relevant geometries that would be challenging to handle by previous methods.

Acknowledgements. We are grateful to T. Emig for providing the raw data from Ref. 12. The authors acknowledge the support of the Interconnect Focus Center, one of five research centers funded under the Focus Center Research Program, a DARPA and Semiconductor Research Corporation program. In addition, the authors are grateful for support from the Singpore-MIT Alliance Computational Engineering flagship research program. This work was supported in part by a Department of Energy (DOE) Computational Science Fellowship under grant DE-FG02-97ER25308 (ARW), by the Army Research Office through the ISN under Contract No. W911NF-07-D-0004, and by the MIT Ferry Fund.

[1] S. K. Lamoreaux, Phys. Rev. Lett. **78**, 5 (1997).
[2] G. Bressi, G. Carugno, R. Onofrio, and G. Ruoso, Phys. Rev. Lett. **88**, 041804 (2002).
[3] D. E. Krause, R. S. Decca, D. Lopez, and E. Fischbach, Phys. Rev. Lett. **98**, 050403 (2007).
[4] H. B. Chan et al., Phys. Rev. Lett. **101**, 030401 (2008).
[5] T. Ederth, Phys. Rev. A **62**, 062104 (2000).
[6] R. Ardito et al., IEEE Sensors 2008 Conference p. 90 (2008).
[7] F. Capasso, J. N. Munday, D. Iannuzzi, and H. B. Chan, IEEE. J. Select. Topic Quantum Electron. **13**, 400 (2007).
[8] J.-G. Guo and Y.-P. Zhao, J. Microelectromechanical Systems **13**, 1027 (2004).
[9] E. Ollier et al., IEEE International Conference on Nano/Micro Engineering and Molecular Systems, Bankkok, Thailand, 16-19 Jan. 2007 p. 180 (2007).
[10] H. B. G. Casimir, Koninkl. Ned. Adak. Wetenschap. Proc. **51**, 793 (1948).
[11] A. W. Rodriguez, M. Ibanescu, D. Iannuzzi, J. D. Joannopoulos, and S. G. Johnson, Phys. Rev. A **76**, 032106 (2007).
[12] T. Emig, N. Graham, R. L. Jaffe, and M. Kardar, Phys. Rev. Lett. **99**, 170403 (2007).
[13] S. Pasquali and A. C. Maggs (2008), arXiv:0801.4385.
[14] A. Lambrecht and V. N. Marachevsky, Phys. Rev. Lett. **101**, 160403 (2008).
[15] H. Gies and K. Klingmüller, Phys. Rev. Lett. **97**, 220405 (2006).
[16] A. Rodriguez et al., Phys. Rev. Lett. **101**, 190404 (2008).
[17] A. W. Rodriguez, J. D. Joannopoulos, and S. G. Johnson, Phys. Rev. A **77**, 062107 (2008).
[18] T. Emig, N. Graham, R. L. Jaffe, and M. Kardar (2008), arXiv:0811.1597.
[19] C. Geuzaine and J.-F. Remacle, Int. J. Numer. Methods Eng. (2009), in press.
[20] S. M. Rao, D. R. Wilton, and A. W. Glisson, IEEE Trans. Antennas Propagat. **AP-30**, 409 (1982).
[21] T. S. Ahmadi, Z. L. Wang, T. C. Green, A. Henglein, and M. A. El-Sayed, Science **272**, 1924 (1996).
[22] R. Jin, Y. Cao, C. A. Mirkin, K. L. Kelly, G. C. Schatz, and J. G. Zheng, Science **294**, 1901 (2001).
[23] H. Li and M. Kardar, Phys. Rev. Lett. **67**, 3275 (1991).
[24] S. Weinberg, *The Quantum Theory of Fields, Vol. 1* (Cambridge University Press, 1995), chapter 9.
[25] S.-H. Kuo, B. Tidor, and J. White, J. Emerg. Technol. Comput. Syst. **4**, 1 (2008), ISSN 1550-4832.
[26] D. J. Taylor, IEEE Trans. Antennas Propagat. **51**, 1630 (2003).
[27] T. Emig, Europhys. Lett. **62**, 466 (2003).
[28] Z. Zhu, B. Song, and J. White, in *Proceedings of the Design Automation Conference* (Anaheim, CA, 2003), pp.

712 –717.
[29] V. Rokhlin, Journal of Computational Physics **60**, 187 (1985).
[30] W. Hackbusch and Z. P. Nowak, Numerische Mathematik **54**, 463 (1989).
[31] J. Schwinger, L. L. DeRaad, Jr, and K. A. Milton, Ann. Phys. **115**, 1 (1978).
[32] Equation (1) is for the zero-temperature case; at finite T the κ integral becomes a sum over Matsubara frequencies [31].